Article

Not peer-reviewed version

Polar Stratospheric Clouds Observations at Concordia Station by the Remotely Controlled Lidar Observatory

Luca Di Liberto , Francesco Colao , Federico Serva , Alessandro Bracci , Francesco Cairo , Marcel Snels *

Posted Date: 26 March 2024

doi: 10.20944/preprints202403.1494.v1

Keywords: climate; ozone; stratosphere; polar stratospheric clouds; lidar

Article

Polar Stratospheric Clouds Observations at Concordia Station by the Remotely Controlled Lidar Observatory

Luca Di Liberto [1], Francesco Colao [2], Federico Serva [3], Alessandro Bracci [1], Francesco Cairo [1] and Marcel Snels [1,*]

[1] CNR-Institute of Atmospheric Sciences and Climate, Via Fosso del Cavaliere 100, 00133 Roma (Italy); l.diliberto@isac.cnr.it (L.D.L.); f.cairo@isac.cnr.it (F.C.)
[2] ENEA, Via Enrico Fermi 45, 00044 Frascati (Italy); francesco.colao@enea.it
[3] CNR-ISMAR,Via Fosso del Cavaliere 100, 00133 Roma(Italy); federico.serva@ismar.cnr.it
* Correspondence:m.snels@isac.cnr.it; Tel.: +39-649934316

Abstract: Polar stratospheric clouds (PSCs) form in polar regions typically between 15 and 25 km, when the local temperature is sufficiently low. PSCs play an important role in the ozone chemistry and the dehydration and denitrification of the stratosphere. Lidars with a depolarization channel may be used to detect and classify different classes of PSCs. The main PSC classes are water ice, nitric acid trihydrate (NAT) and supercooled ternary solutions (STS), the latter being liquid droplets consisting of water, nitric acid and sulphuric acid. PSCs have been observed at the lidar observatory at Concordia Station from 2014 on. The harsh environmental conditions at Concordia during winter render successful lidar operation difficult. In order to facilitate the operation of the observatory several measures have been put in place to achieve an almost complete remote control of the system. PSC occurrence is strongly correlated with local temperatures and is affected by dynamics, as the PSC coverage during the observation season shows.

Keywords: climate; ozone; stratosphere; polar stratospheric clouds; lidar

1. Introduction

The first sightings of polar stratospheric clouds have been reported in the late 19^{th} century. Because of their brilliant colours they were called nacreous clouds or mother-of-pearl clouds. Later on it was discovered that they formed in the stratosphere, at very cold conditions.

Only after the discovery of the ozone hole, polar stratospheric clouds gained major attention, being held responsible for catalizing the ozone distruction by chlorofluorocarbons (CFCs). The scientific observation of PSCs started around 1990 with ground-based lidars (McMurdo, Dumont D'Urville, South Pole) and in the 21th century with satellite borne lidars. From the beginning two types of PSCs were distinguished, type II, forming below the ice frost point around -83^{o}C, consisting of water ice and exhibiting the the bright colours of mother-of-pearl, and type I, that were observed aso at warmer temperatures. These were divided in sub-classes, with different chemical composition. One sub-class is formed by liquid supercooled particles composed of water, nitric acid and sulphuric acid (STS, supercooled ternary solutions). These particles have spherical symmetry and thus don't depolarize the laser light. A second sub-class is formed by water and nitric acid, typically with a stoichiometry of 3:1 (nitric acid trihydrate, NAT). A third sub-class collects a number of nitric acid hydrates of different composition. Both NAT and other nitric acid hydrates are solid particles and thus cause a depolarization of the laser light. Externally mixed clouds with intemediate characteristis are also often observed.

Lidars with a receiver equipped with two channels to separate polarized and depolarized signals (see eg [1] for a review of polarization lidars) are thus an excellent tool to allow a classification of the different PSC types and sub-classes. Ground-based lidars have been active in Antarctica since 1987, and in the Artic polar regions since 1989. Krüger [2] reported lidar observations at Ny-Alesund/Svalbard in 1989. The first lidar measurements in Antarctica were reported by Fiocco and coworkers [3] who reported the observation of PSCs at the South Pole station, using a laser emitting at 532 nm without depolarization channel. Stefanutti [4] reported lidar observations at Dumont D'Urville from 1989 to

 doi:10.20944/preprints202403.1494.v1

1993. Recent PSC observations at Dumon D'Urville have been reported in [5]. A polarization lidar has been active at McMurdo from 1989 up to 2010 [6,7], and has been transferred to Concordia Station in 2014 [8]. A combination of simultaneous lidar and balloon borne optical particle counter measurements allows to compare size distribution with the obsered optical properties of aerosol present in PSCs [9,10].

Very few stratospheric lidars have been operating in the Antarctic and only two of these are primary lidar stations of the Network of Atmospheric Composition Change (NDACC). These are located at Dumont D'Urville and at Concordia Station. In a recent study [11] Concordia Station has been identified as one of the best locations for observing Polar Stratospheric Clouds (PSCs). One reason is the limited cloud cover by cirrus clouds, which might partly block the lidar and reduce the useful range for PSCs. Moreover, Concordia Station is well within the polar vortex during most of the austral winter, which implies that the conditions for PSC formation are favourable, leading to a frequent occurrence.

Operating a lidar in Antarctic presents additional problems with respect to a lidar at mid-latitude locations. This is mainly due to the remoteness of the Station and the harsh environmental conditions, which render technical adjustments and maintenance difficult. This is mitigated by the redundance of the most important components of the lidar, such as the laser and optical systems, as well as the data acquisition modules. Technicians and scientists which run the observatory and many other experiments, have to be instructed during the summer campaign and often have no prior experience with lasers and lidars. However, they are essential for running the system, acquiring data, cleaning the view window and other tasks. During the last few years the lidar alignment and data acquisition can be performed remotely. This implies that the technicians can remain in their office to operate the observatory, without having to go outside at temperatures which can be as low as -70^{o}C with bad visibility and strong winds to reach the observatory at a distance of 300-400 m. If necessary, the lidar can be remotely controlled from our Institute in Italy.

2. Materials and Methods

2.1. Description of the Remote Controlled Lidar

Concordia Station is a French–Italian research facility that was built in 2005, located on the Antarctic Plateau at 3233 m above sea level (75.1^{o}S 123.3^{o}E, see Figure 1). Its position at the Antarctic Plateau, about 1100-1200 km from the French research station at Dumont D'Urville, Australia's Casey Station and the Italian Zucchelli Station at Terra Nova Bay, all of them coastal stations, makes it a unique location for the observation of polar stratospheric clouds. Concordia is operational throughout the year, with a winter staff of about 15 technicians and scientists.

The lidar observatory at Concordia Station has been active since 2014. The main equipment was already deployed at McMurdo Station from 2004 to 2010 [7]. However, many components have been upgraded and added to increase the reliability, the redundancy, to improve the data quality and extend the measurement range. The remote control of data acquisition, setting of system parameters and laser alignment have been implemented in last four years. The lidar observatory uses a compact Quantel Big Sky laser (model CFR400) emitting at two wavelengths at a 10 Hz repetition rate, with a pulse energy of about 180 mJ at 532 nm and 100 mJ at 1064 nm. Two receivers are used to collect the scattered light. A Schmidt Cassegrain telescope (Celestron model C14-AF XLT) with a diameter of 14 inch (355.6 mm) is used for the observation of PSCs at ranges between 10 and 30 km, while a smaller 6 inch (152.4 mm) telescope (xxx model yyy) is used to observe tropospheric clouds. The larger receiver is coupled to an optical box where the optical signal is separated in different components and detected by miniaturized photomultipliers (Hamamatsu models H6780-20, H5783P and H10721P-210) for the optical wavelengths or by an avalanche photo diode (APD, EG&G, Perkin-Elmer model SPCM-AQR-14) for the infrared signal. Details of the optical system can be found in [12]. The output of the optical detectors is fed into a photon-counting system (ALA Systems, model APC26 main) with ten available channels, thus offering some redundacy for the 7 detectors. The parameters of the photon counting system, including dwell time, number of averages, pretrigger etc can be remotely controlled

 doi:10.20944/preprints202403.1494.v1

and the lidar profiles are automatically stored on a local computer and transmitted to a dedicated server in Italy. The local computer can be accessed from remote and allows the control of the laser, the photon-counting system, the data storage and transmission as well as the control of the laser alignment. The laser alignment is obtained by a piezo-controlled mirror which can be scanned in azimuth and tangent angles with respect to the axis of the large telescope. A dedicated computer program in Python provides an automatic alignment procedure by scanning the two angles with respect to a starting point and acquires the lidar signal at each setting, thus creating an intensity map by integrating the amplitude of the return signal (in photon counts) between predetermined altitudes. The maximum signal of this map becomes a new starting point and the process is repeated until the optimum signal is obtained. In alternative the piezo controlled mirror can be accessed directly by the operator to find the best conditions "manually". The laser parameters can be accessed remotely, which allows to optimize laser intensity and to monitor the state of the flashlamps. See Figure 2 for schematic view of the remotely controlled hardware.

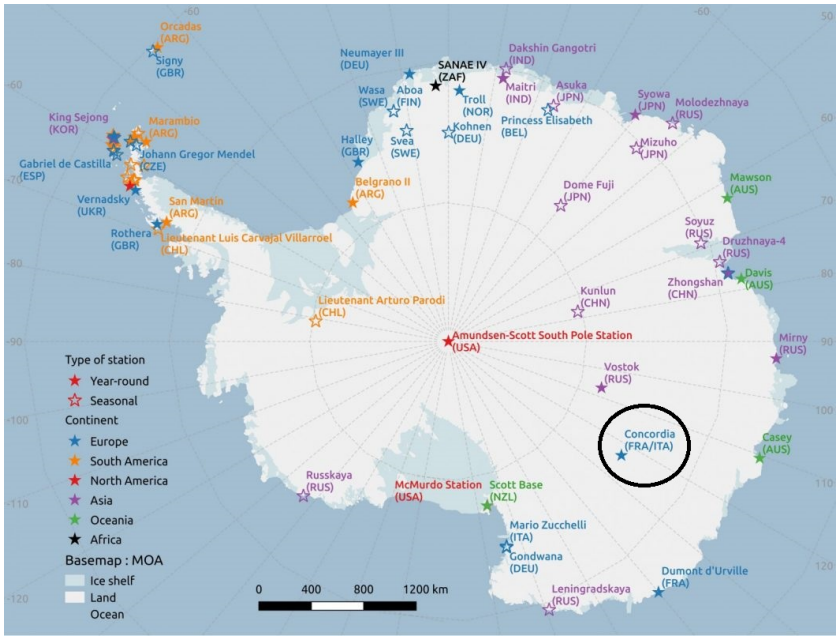

Figure 1. The figure shows a map of Antarctica, with the position of Concordia Station with respect to other bases.

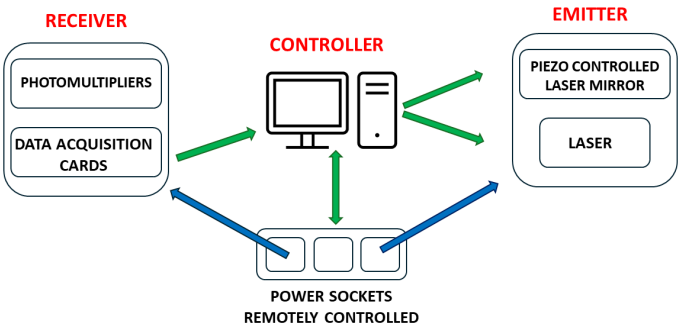

Figure 2. The figure shows a schematic view of the remote control.

 doi:10.20944/preprints202403.1494.v1

2.2. Description of the Measurement Methods

A satellite borne lidar (CALIOP, Cloud Aerosol Lidar with Orthogonal Polarization) on the CALIPSO (Cloud-Aerosol Lidar and Infrared Pathfinder Satellite Observations) satellite was active from 2006 to 2023. CALIPSO was part of the A-train and with an orbit inclination of 98.2°, it provided extensive daily measurement coverage over the polar regions of both hemispheres, up to 82° in latitude, with 14 or 15 orbits per day. Most measurements at Concordia station were made in coincidence with CALIPSO overpasses, having footprints at distances smaller than 200 km from Concordia station. This results in a few quasi-coincidences per day (see also [7] and [8]). These coincident measurements allowed comparison of ground-based and satellite-borne instruments for a large data set of PSC observations. Usually measurements were performed starting 16 minutes before the overpass and terminating 16 minutes after the overpass, in intervals of 2 minutes. This allowed to observe the observation of variations in the PSC observations on the time scale of minutes, which is usefull to obtain information about the extension of PSC clouds, taking into account the windspeed at different altitudes.

2.3. Preprocessing of the Raw Lidar Data

Raw data consist of photon counts recorded in 400 ns bins, corresponding with a vertical resolution of 60 m. Data are recorded and averaged in 2 minute intervals. The laser is emitting, within a good approximation, linearly polarized light at 532 nm. The molecules and particles in the air may partly depolarize the reflected light. The main constituents of the atmosphere are oxygen and nitrogen molecules, which reflect mainly polarized light, with a small fraction of depolarized light. Particles with a spherical symmetry (liquid drops) do not depolarize the reflected light, while solid particles reflect both polarized and depolarized radiation. Thus measuring two orthogonal polarizations of the reflected light provides information about the physical (and chemical) properties of the aerosol particles. A set of polarizing beamsplitter cubes is used to separate two polarizations, one with a polarization parallel to the emitted laser beam, the second orthogonal to it. Here we consider the preprocessing of the raw optical signals of the two polarizations (parallel and perpendicular). Both signals are attenuated by the molecules and particles in the air, and a correction is applied to compensate for this attenuation, by using a simplified version of the Klett method [13], by using a fixed lidar ratio of 70, which appears appropriate for PSCs. We tested this fixed lidar ratio on a large number of lidar profiles and obtained satisfactory results, while the variable lidar ratio used in previous work [12], using the results of a number of model calculations for several particle size distributions [14] (runs 86 and 99) produced less satisfactory results, leading to a significant underestimation of the extinction compared to the method proposed by Young and Vaughan [15].

Unfortunately the two recorded channels with orthogonal polarization do not fully represent the polarization of the lidar signal, but suffer from crosstalk between the two polarization components. In particular the perpendicular channel suffers from contributions which are not produced by the depolarization by molecules and aerosol. The imperfect polarization of the laser emission contributes to a small signal on the perpendicular channel, but is usually smaller than 1 %. Also the imperfect behaviour of the two polarizing beamspliiter cubes introduces some crosstalk. Normally the crosstalk of a polarizing beamspliiter cube might be as large as 5%, but the combination of two cubes reduces this to less than 1 %. Also the non-perfect collimation of the optical return signal might contribute. A thorough discussion of the various factors which might contribute to crosstalk, as well as a method to calibrate the receiver with two polarizations can be found in [16]. However, in the case of the lidar observatory at Concordia station, the main contribution to the crosstalk is produced by the depolarization of the return signal by the optical viewport. This viewport, which is separating the laboratory environment at room temperature (normally between 15 and 20 ^{0}C) from the outside air, with temperatures which might be a low as -70^{0}C, consists of a triple glass construction, with three panes of glass held together in a glazing unit with two insulating air gaps with a distance of about

 doi:10.20944/preprints202403.1494.v1

10 cm between two panes. This is necessary to provide a sufficient thermal insulation, and functions quite well, but apparently causes a depolarization of the lidar signal which amounts to about 14 %.

After correcting the two channels for extinction and range, two optical parameters can be extracted, taking into account the crosstalk. A more detailed description of the processing of the raw data can be found in [8]. The backscatter ratio R, defined as the ratio of the total backscatter coefficient and the molecular backscatter coefficient, accounts for the scattering by particles (aerosol) with respect to molecular scattering. This implies that R =1 if no aerosols are present. The second parameter accounts for the depolarization caused by solid particles and can be described by several parameters [17]. The linear volume depolarization is defined as the ratio of the perpendicular backscatter coefficient and the parallel backscatter coefficient, while the aerosol depolarization can be expressed as the ratio of the perpendicular backscatter coefficient and the parallel backscatter coefficient for aerosol only. We use the perpendicular backscatter coefficient $\beta_{\perp}$ as a measure for depolarization, to facilitate the comparison with CALIOP data.

The determination of the two optical parameters, R and $\beta_{\perp}$ and their errors, allow to define detection limits and to classify the different PSC classes.

2.4. Detection and Classification of PSCs

In a previous work [8] an extensive comparison study of ground-based and quasi-coincident satellite-borne lidar observations of PSCs was performed. In order to make this comparison we had to adopt a detection and classification algorithm which follows the same approach and uses the same optical parameters as the v2 CALIOP algorithm (see Figure 3 and [7,18]). However, the detection thresholds to distinguish PSCs from background aerosol had to be calculated in a different way. For CALIOP observations the signal due to background aerosol from measurements is determined from observations at different locations on the same orbit, where no PSCs are present. For the ground-based observations the background aerosol signal is taken from apparent clear sky observations, which are far less than PSC observations during winter and often at different times with respect to the PSC observations.

Furthermore, statistical errors inherent of the photon counting process and thus depending on the altitude and on the possible attenuation in the lower troposphere, have been taken into account to calculate the errors of the optical parameters u($\beta_{\perp}$) and u(R) and create the dynamic thresholds for detection and classification.

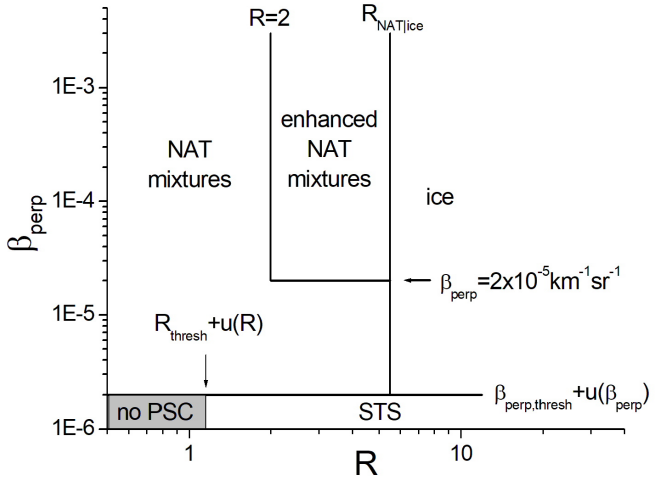

Figure 3. The figure shows the criteria using R and β_{perp} to classify the different PSC types.

 doi:10.20944/preprints202403.1494.v1

The detection of a PSC is positive if either R or $\beta_{\perp}$ exceeds the threshold value. It should be noted that the threshold values are not fixed but vary with the altitude, due to the variation of the signal-to-noise ratio of the measured parameters. The classification of the PSCs closely follows the criteria established for the CALIOP data, and identifies 5 different classes, STS (Supercooled Ternary Solutions), NAT (Nitric Acid Trihydrates) mixtures, enhanced NAT, ice and wave ice. With the term NAT mixtures we intend mixtures of NAT with STS and other non polarizing particles. PSC clouds generally consist of external mixtures of different species. The classification is based on the measurement of optical parameters and as such on the average contribution of several species to backscatter coefficient and depolarization. Enhanced NAT particles correspond to NAT with $r_{NAT} < 3$ μm and a volume density of more than 1 $\mu m^3 cm^{-3}$ [18] and corresponds roughly with NAT heterogeneously nucleated in wave ice PSCs. Wave ice PSCs are ice PSCs with $R > 50$. Wave ice seldom occurs above Concordia, since no significant orographic features are present. Also enhanced NAT has a low occurrence. The main PSC classes observed at Concordia Station are NAT, STS and ice.

3. Results and Discussion

The Concordia lidar observatory has been active since 2014. Lidar profiles have been recorded during the months of major PSC occurrences, from June through September. Usually 2 to 4 profiles have been recorded every day, with exception of prohibitive meteo conditions, such as storm, precipitation or strongly absorbing tropospheric clouds. In 2019 both lasers broke down and no data acquisitions were possibile. Here we show the PSC observations performed in 2021, as an example of the seasonal variations of the PSC occurrences.

The formation of PSCs is mainly dictated by temperature, since the different kinds of PSCs exist in a limited temperature range (see e.g., [19–21]). Above a certain threshold temperature they simply evaporate and cease to exist as solid or liquid particles. On the other hand the formation processes can follow different pathways, depending on temperature history induced by either large synoptic fields or mesoscale features. The upper temperature threshold for PSCs is the formation temperature for NAT (T_{NAT}) which is around 195 K, depending on the water vapor and nitric acid mixing ratios, local pressure and temperatures [22]. T_{NAT} is the highest PSC formation temperature that is thermodynamically possible, but usually NAT forms at about 2.5-3 K below T_{NAT} [18]. Water-ice PSCs have the lowest formation temperature (about 188 K), the so-called frost temperature (see e.g. [23] or [24] for different methods to calcuate the frost point).

The nucleation and growth of the different PSCs has been extensively discussed elsewhere [25]. The abundance of water in the troposphere and stratosphere, with respect to nitric acid, sulphuric acid and other condensable species, produces ice PSCs when the local temperature is low enough. Homogeneous ice nucleation from SSA (Supercooled sulphuric acid) or from STS occurs typically at T_{ice}-4 K [26–28], while heterogeneous nucleation on NAT particles, occurs already below T_{ice}, but above T_{ice}-4 K [29,30].

For the formation of NAT particles several pathways have been proposed [31]. The heterogeneous nucleation on ice particles requires that the temperature should be low enough to produce ice PSCs, implying that other formation processes are required for $T>T_{ice}$.

The heterogeneous nucleation on background aerosols containing meteoritic material [32], or other condensation nuclei might occur readily below T_{NAT} however. The possibility of homogeneous nucleation on STS iwas rejected by [28].

Liquid STS droplets, being ternary solutions with a variable stoichiometry, do not form below a definite threshold temperature but rather grow by a continuous uptake of nitric acid by sulphuric acid aerosols, which becomes massive below 195 K [33]. The composition of the STS droplets changes with temperature; while temperature decreases, the HNO_3 concentration increases, while the H_2SO_4 concentration decreases.

The formation of PSCs causes a depletion of water and nitric acid in the gas phase, which leads to a dehydration and denitrification of the stratosphere.

 doi:10.20944/preprints202403.1494.v1

3.1. PSC Observations in 2021

We can observe in Figure 4, reporting the PSC observatons during 2021, that PSC are seldom observed when the local temperature exceeds T_{NAT}-3K. E.g. during the first 10 days of June, the temperature below 14-16 km is too high to allow formation of PSCs. Also very few PSCs can be observed above 26 km, where the temperature is too high. The red contours, indicating T_{ice} enclose favourable conditions for ice PSC formation, and it can be observed that ice PSC are observed below T_{ice}, but it is clear that $T<T_{ice}$ is a necessary condition but not a sufficient condition for ice PSC formation. With respect to previous years, the 2021 polar vortex was rather cold, as can be seen in Figure 4, where large areas of temperatures below T_{ice} can be observed. Until the end of June, temperatures are too high for ice PSCs to form, and we see mainly NAT mixture, where NAT is formed by heterogeneous nucleation on background aerosol or other condensation nuclei. In July and August ice PSCs are often observed, in correspondence with temperatures below 185 K. The formation of ice PSCs leads to dehydratation which can also be observed in MLS measurements of the water vapour mixing ratio (see Figure 5. At temperatures below T_{ice}, the coexistence of ice, NAT mixtures and STS can be observed.

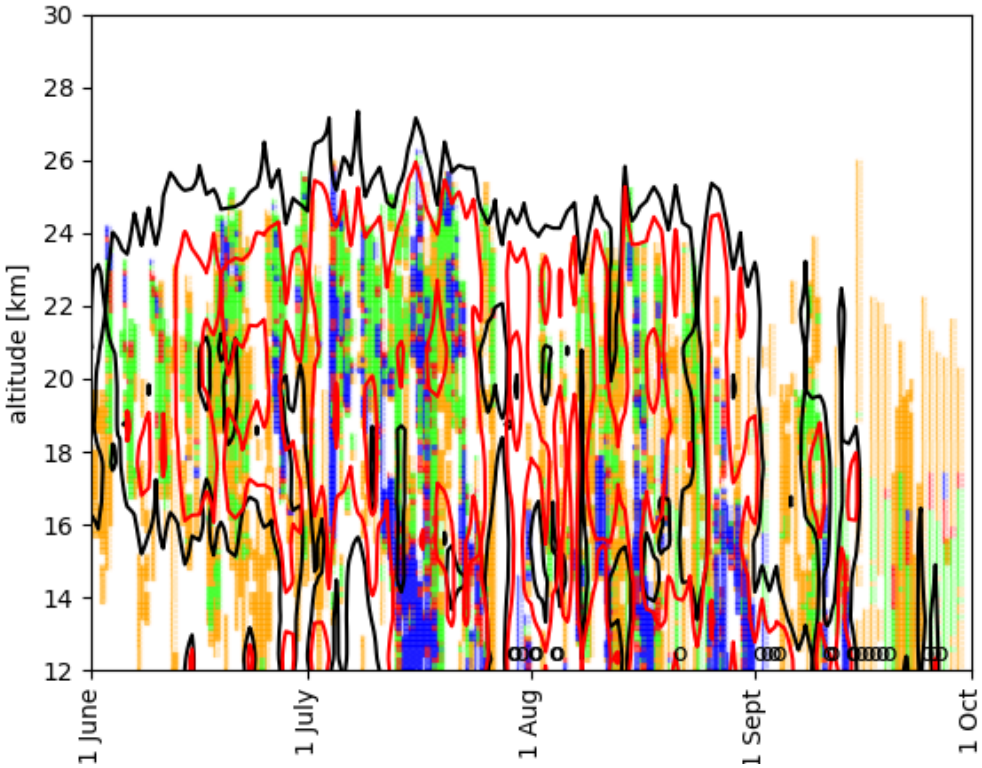

Figure 4. The figure shows the PSCs observed in 2021. The black contour corresponds with T_{NAT}-3K while the red contours indicate the ice PSC formation temperature. The formation temperatures have been calculated from local pressure and water vapour and nitric acid mixing ratios obtained from MLS data.

The ubiquitous presence of STS in September is somewhat surprising, considering the temperature maps. PSCs are seldom observed by CALIOP in September above Concordia [8], but this may be due to a minor sensitivity with respect to the ground-based lidar. On the other hand it might be partially an instrumental effect, due to the presence of sunlight causing baseline fluctuations, which has a major effect on the weaker depolarized signal.

 doi:10.20944/preprints202403.1494.v1

In conclusion the 2021 PSC observations illustrate the important role of temperature in the PSC formation process and it confirms some of the proposed formation pathways, in particular concerning the NAT formation in June.

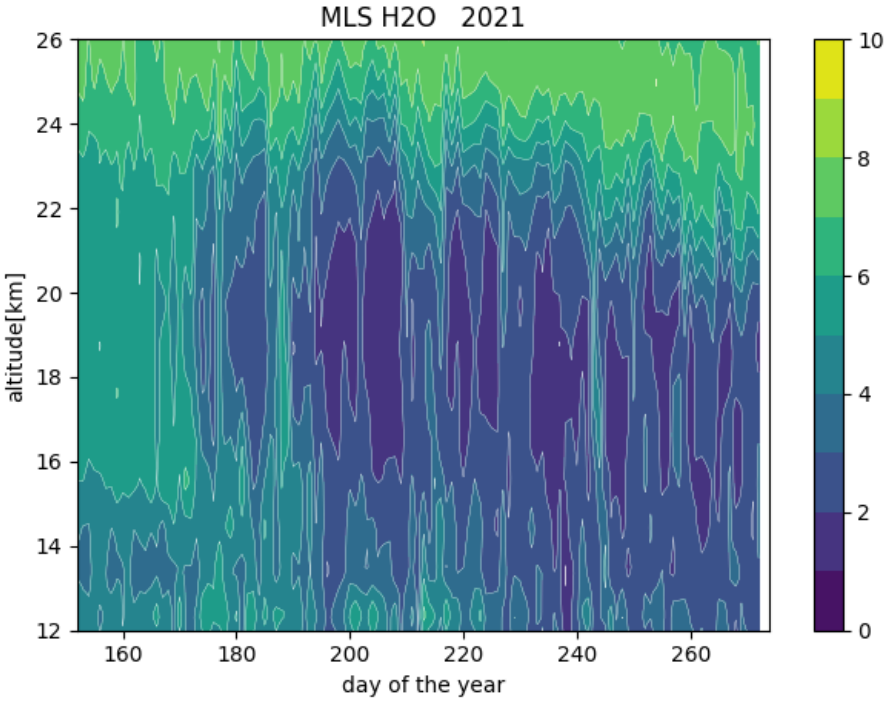

Figure 5. The figure shows the water vapour mixing ratio in ppm as observed by MLS in 2021.

Author Contributions: Conceptualization, M.S., L.DL and F.Ca.; methodology, M.S., L.DL and F.Co.; software, F.Co, M.S. and F.S..; validation, L.DL, A.B and F.S..; formal analysis,L.DL , M.S. and F.S..; investigation, F.Ca, A.B. and F.Co..; resources, M.S. and F.Co.; data curation, L.Dl and M.S..; writing—original draft preparation, M.S and L.DL. .; writing—review and editing, all authors.; visualization, all authors; supervision, M.S. .; project administration, M.S.; funding acquisition, M.S. and F.Co. All authors have read and agreed to the published version of the manuscript.", please turn to the CRediT taxonomy for the term explanation. Authorship must be limited to those who have contributed substantially to the work reported.

Funding: This research was funded by the Piano Nazionale della Ricerca in Antartide (PNRA) in the frame work of the projects 2009/B.08 and OSS-12.

Data Availability Statement: The raw lidar data are available from the NDACC website : https://www-air.larc.nasa.gov/missions/ndacc/data.html?station=dome.c/ames/lidar/.

Acknowledgments: The authors acknowledge the financial support by PNRA in the frame work of the projects 2009/B.08 and OSS-12. We also acknowledge the support of the ISSI-PSC initiative project. Logistical and winter-time technical support was provided by the Programma Nazionale delle Ricerche in Antartide (PNRA). The authors thank Igor Petenko, Giampietro Casasanta, Simonetta Montaguti, Alfonso Ferrone, Filippo Cali Quaglia, Meganne Christian, Alberto Salvati, Rodolfo Canestrari, Angelo Galeandro and Davide Carlucci for performing the ground-based lidar measurements at Dome C during the winter and Maurizio Viterbini and Ilir Shuli for their valuable technical support. A particular mention goes to Luca Iannello, winterover 2020, for enabling the remote control via VPN, thus providing remote alignment of the lidar, which improved the the quality of the measurements.

Conflicts of Interest: The authors declare no conflict of interest. The funders had no role in the design of the study; in the collection, analyses, or interpretation of data; in the writing of the manuscript; or in the decision to publish the results.

Abbreviations

The following abbreviations are used in this manuscript:

 doi:10.20944/preprints202403.1494.v1

PSC	Polar Stratospheric Cloud
LIDAR	LIght Detecting And Ranging
CALIOP	Cloud-Aerosol Lidar with Orthogonal Polarization
CALIPSO	Cloud-Aerosol Lidar and Infrared Pathfinder Satellite Observation
NAT	Nitric Acid Trihydrate
STS	Supercooled Ternary Solution
MLS	Microwave Limb Sounder
PNRA	Programma Nazionale delle Ricerche in Antartide
NDACC	Network for the Detection of Stratospheric Change

References

1. Sassen, K. The Polarization Lidar Technique for Cloud Research: A Review and Current Assessment. *Bulletin of the American Meteorological Society* **1991**, *72*, 1848 – 1866. doi:10.1175/1520-0477(1991)072<1848:TPLTFC>2.0.CO;2.
2. Krueger, B.C. Observations of polar stratospheric clouds in the Arctic winter 1989 at 79 N. *Geophysical Research Letters* **1990**, *17*, 365–368. doi:10.1029/GL017i004p00365.
3. Fiocco, G.; Cacciani, M.; Di Girolamo, P.; Fua, D. Stratospheric clouds at South-Pole during 1988 .1. Results of lidar observations and their relationship to temperature. *Journal of Geophysical Research-Atmospheres* **1992**, *97*, 5939–5946.
4. Stefanutti, L.; Morandi, M.; Guasta, M.D.; Godin, S.; Megie, G.; Brechet, J.; Piquard, J. Polar stratospheric cloud observations over the Antarctic continent at Dumont d'Urville. *Journal of Geophysical Research: Atmospheres* **1991**, *96*, 12975–12987. doi:https://doi.org/10.1029/91JD00776.
5. Tencé, F.; Jumelet, J.; Bouillon, M.; Cugnet, D.; Bekki, S.; Safieddine, S.; Keckhut, P.; Sarkissian, A. 14 years of lidar measurements of polar stratospheric clouds at the French Antarctic station Dumont d'Urville. *Atmospheric Chemistry and Physics* **2023**, *23*, 431–451. doi:10.5194/acp-23-431-2023.
6. Adriani, A.; Massoli, P.; Di Donfrancesco, G.; Cairo, F.; Moriconi, M.; Snels, M. Climatology of polar stratospheric clouds based on lidar observations from 1993 to 2001 over McMurdo Station, Antarctica. *Journal of Geophysical Research-Atmospheres* **2004**, *109*. doi:{10.1029/2004JD004800}.
7. Snels, M.; Scoccione, A.; Di Liberto, L.; Colao, F.; Pitts, M.; Poole, L.; Deshler, T.; Cairo, F.; Cagnazzo, C.; Fierli, F. Comparison of Antarctic polar stratospheric cloud observations by ground-based and spaceborne lidars and relevance for chemistry-climate Models. *Atmospheric Chemistry and Physics* **2019**, pp. 955–972. doi:10.5194/acp-19-955-2019.
8. Snels, M.; Colao, F.; Cairo, F.; Shuli, I.; Scoccione, A.; De Muro, M.; Pitts, M.; Poole, L.; Di Liberto, L. Quasi-coincident observations of polar stratospheric clouds by ground-based lidar and CALIOP at Concordia (Dome C, Antarctica) from 2014 to 2018. *Atmospheric Chemistry and Physics* **2021**, *21*, 2165–2178. doi:10.5194/acp-21-2165-2021.
9. Snels, M.; Cairo, F.; Di Liberto, L.; Scoccione, A.; Bracaglia, M.; Deshler, T. Comparison of Coincident Optical Particle Counter and Lidar Measurements of Polar Stratospheric Clouds Above McMurdo (77.85°S, 166.67°E) From 1994 to 1999. *Journal of Geophysical Research: Atmospheres* **2021**, *126*, e2020JD033572. e2020JD033572 2020JD033572, doi:https://doi.org/10.1029/2020JD033572.
10. Cairo, F.; Deshler, T.; Di Liberto, L.; Scoccione, A.; Snels, M. A study of optical scattering modelling for mixed-phase polar stratospheric clouds. *Atmospheric Measurement Techniques* **2023**, *16*, 419–431. doi:10.5194/amt-16-419-2023.
11. Tesche, M.; Achtert, P.; Pitts, M.C. On the best locations for ground-based polar stratospheric cloud (PSC) observations. *Atmospheric Chemistry and Physics* **2021**, *21*, 505–516. doi:10.5194/acp-21-505-2021.
12. Di Liberto, L.; Cairo, F.; Fierli, F.; Di Donfrancesco, G.; Viterbini, M.; Deshler, T.; Snels, M. Observation of polar stratospheric clouds over McMurdo (77.85^{o}S, 166.67^{o}E) (2006-2010). *Journal of Geophysical Research: Atmospheres* **2014**, *119*, 5528–5541. doi:https://doi.org/10.1002/2013JD019892.
13. Klett, J. Lidar Inversion with Variable Backscatter/Extinction Ratios. *Applied Optics* **1985**, *24*, 1638–1643. doi:https://doi.org/10.1364/AO.24.001638.
14. Gobbi, G. Lidar estimation of stratospheric aerosol properties - surface, volume, and extinction to backscatter ratio. *Journal of Geophysical Research-Atmospheres* **1995**, *100*, 11219–11235. doi:{10.1029/94JD03106}.

15. Young, S.A.; Vaughan, M.A. The Retrieval of Profiles of Particulate Extinction from Cloud-Aerosol Lidar Infrared Pathfinder Satellite Observations (CALIPSO) Data: Algorithm Description. *Journal of Atmospheric and Oceanic Technology* **2009**, *26*, 1105 – 1119. doi:10.1175/2008JTECHA1221.1.
16. Snels, M.; Cairo, F.; Colao, F.; Di Donfrancesco, G. Calibration method for depolarization lidar measurements. *International Journal of Remote Sensing* **2009**, *30*, 5725–5736. doi:{10.1080/01431160902729572}.
17. Cairo, F.; Donfrancesco, G.D.; Adriani, A.; Pulvirenti, L.; Fierli, F. Comparison of various linear depolarization parameters measured by lidar. *Appl. Opt.* **1999**, *38*, 4425–4432. doi:10.1364/AO.38.004425.
18. Pitts, M.C.; Poole, L.R.; Gonzalez, R. Polar stratospheric cloud climatology based on CALIPSO spaceborne lidar measurements from 2006–2017. *Atmospheric Chemistry and Physics* **2018**, *2018*, 10881–10913. doi:10.5194/acp-18-10881-2018.
19. Tabazadeh, A.; Toon, O.; Hamill, P. Freezing behaviour of stratospheric sulfate aerosols inferred from trajectory studies. *Geophysical Research Letters* **1995**, *22*, 1725–1728. doi:{10.1029/95GL01335}.
20. Larsen, N.; Knudsen, B.; Rosen, J.; Kjome, N.; Neuber, R.; Kyro, E. Temperature histories in liquid and solid polar stratospheric cloud formation. *Journal of Geophysical Research-Atmospheres* **1997**, *102*, 23505–23517. doi:{10.1029/97JD01666}.
21. Toon, O.; Tabazadeh, A.; Browell, E.; Jordan, J. Analysis of lidar observations of Arctic polar stratospheric clouds during January 1989. *Journal of Geophysical Research-Atmospheres* **2000**, *105*, 20589–20615. doi:{10.1029/2000JD900144}.
22. Hanson, D.; Mauersberger, K. Laboratory studies of the nitric acid trihydrate: Implications for the south polar stratosphere. *Geophysical Research Letters* **1988**, *15(8)*, 855–858. doi:10.1029/GL015i008p00855.
23. Murphy, D.M.; Koop, T. Review of the vapour pressures of ice and supercooled water for atmospheric applications. *Quart. J. Roy. Meteor. Soc.* **2005**, *131*, 1539–1565. doi:https://doi.org/10.1256/qj.04.94.
24. Romps, D.M. Accurate Expressions for the Dewpoint and Frost Point Derived from the Rankine–Kirchhoff Approximations. *Journal of the Atmospheric Sciences* **2021**, *78*, 2113 – 2116. doi:10.1175/JAS-D-20-0301.1.
25. Tritscher, I.; Pitts, M.C.; Poole, L.R.; Alexander, S.P.; Cairo, F.; Chipperfield, M.P.; Grooß, J.U.; Höpfner, M.; Lambert, A.; Luo, B.; Molleker, S.; Orr, A.; Salawitch, R.; Snels, M.; Spang, R.; Woiwode, W.; Peter, T. Polar Stratospheric Clouds: Satellite Observations, Processes, and Role in Ozone Depletion. *Reviews of Geophysics* **2021**, *59*, e2020RG000702. e2020RG000702 2020RG000702, doi:https://doi.org/10.1029/2020RG000702.
26. Carslaw, K.S.; Wirth, M.; Tsias, A.; Luo, B.P.; Dörnbrack, A.; Leutbecher, M.; Volkert, H.; Renger, W.; Bacmeister, J.T.; Peter, T. Particle microphysics and chemistry in remotely observed mountain polar stratospheric clouds. *Journal of Geophysical Research: Atmospheres* **1998**, *103*, 5785–5796. doi:https://doi.org/10.1029/97JD03626.
27. Koop, T.; Ng, H.P.; Molina, L.T.; Molina, M.J. A New Optical Technique to Study Aerosol Phase Transitions: The Nucleation of Ice from H2SO4 Aerosols. *The Journal of Physical Chemistry A* **1998**, *102*, 8924–8931. doi:10.1021/jp9828078.
28. Koop, T.; Biermann, U.; Raber, W.; Luo, B.; Crutzen, P.; Peter, T. Do stratospheric droplets freeze above the ice frost point ? *Geophysical Research Letters* **1995**, *22*, 917–920. doi:{10.1029/95GL00814}.
29. Koop, T.; Carslaw, K.S.; Peter, T. Thermodynamic stability and phase transitions of PSC particles. *Geophysical Research Letters* **1997**, *24*, 2199–2202. doi:https://doi.org/10.1029/97GL02148.
30. Peter, T. MICROPHYSICS AND HETEROGENEOUS CHEMISTRY OF POLAR STRATOSPHERIC CLOUDS. *Annual Review of Physical Chemistry* **1997**, *48*, 785–822. PMID: 15012456, doi:10.1146/annurev.physchem.48.1.785.
31. Peter, T.; Grooß, J.U. Polar Stratospheric Clouds and Sulfate Aerosol Particles: Microphysics, Denitrification and Heterogeneous Chemistry. In *Stratospheric Ozone Depletion and Climate Change*; The Royal Society of Chemistry, 2012; pp. 108–144. doi:10.1039/9781849733182-00108.
32. Curtius, J. Observations of meteoritic material and implications for aerosol nucleation in the winter Arctic lower stratosphere derived from in situ particle measurements. *Atmos. Chem. Phys. Disc* **2005**, *5*, 5039–5080.
33. Carslaw, K.; Luo, B.; Peter, T. An analytic expression for the composition of acqueous HNO_3-H_2SO_4 stratospheric aerosols including gas-phase removal of HNO_3. *Geophysical Research Letters* **1995**, *22*, 1877–1880. doi:{10.1029/95GL01668}.